Geomagnetic storms, super-storms, and their impacts on GPS-based navigation systems

E. Astafyeva, Yu. Yasyukevich, A. Maksikov, I. Zhivetiev

AGU PUBLICATIONS

Space Weather

RESEARCH ARTICLE
10.1002/2014SW001072

Key Points:
- Super-storms have larger impact on GPS performance than less intense storms
- Global maps of GPS Losses-of-Lock reflect redistribution of ionospheric plasma
- Maps of TEC slips indicate the storm time position of the auroral oval

Supporting Information:
- Readme
- Animation S1
- Animation S2

Correspondence to:
E. Astafyeva,
astafyeva@ipgp.fr

Citation:
Astafyeva, E., Y. Yasyukevich, A. Maksikov, and I. Zhivetiev (2014), Geomagnetic storms, super-storms, and their impacts on GPS-based navigation systems, *Space Weather, 12*, 508–525, doi:10.1002/2014SW001072.

Received 28 MAR 2014
Accepted 9 JUL 2014
Accepted article online 14 JUL 2014
Published online 30 JUL 2014

Geomagnetic storms, super-storms, and their impacts on GPS-based navigation systems

E. Astafyeva[1], Yu. Yasyukevich[2,3], A. Maksikov[3], and I. Zhivetiev[4]

[1]Institut de Physique du Globe de Paris, Paris Sorbonne Cité, Univ. Paris Diderot, UMR CNRS 7154, Paris, France, [2]Institute of Solar-Terrestrial Physics SB RAS, Irkutsk, Russian Federation, [3]Irkutsk State University, Irkutsk, Russian Federation, [4]Institute of Cosmophysical Research and Radiowave Propagation FEB RAS, Petropavlovsk-Kamchatskii, Russian Federation

Abstract Using data of GPS receivers located worldwide, we analyze the quality of GPS performance during four geomagnetic storms of different intensity: two super-storms and two intense storms. We show that during super-storms the density of GPS Losses-of-Lock (LoL) increases up to 0.25% at L1 frequency and up to 3% at L2 frequency, and up to 0.15% (at L1) and 1% (at L2) during less intense storms. Also, depending on the intensity of the storm time ionospheric disturbances, the total number of total electron content (TEC) slips can exceed from 4 to 40 times the quiet time level. Both GPS LoL and TEC slips occur during abrupt changes of SYM-H index of geomagnetic activity, i.e., during the main phase of geomagnetic storms and during development of ionospheric storms. The main contribution in the total number of GPS LoL was found to be done by GPS sites located at low and high latitudes, whereas the area of numerous TEC slips seemed to mostly correspond to the boundary of the auroral oval, i.e., region with intensive ionospheric irregularities. Our global maps of TEC slips show where the regions with intense irregularities of electron density occur during geomagnetic storms and will let us in future predict appearance of GPS errors for geomagnetically disturbed conditions.

1. Introduction

Ionospheric response to a geomagnetic storm, known as an ionospheric storm, is manifested in a large variety of effects and is not well understood yet. Depending on storm time variations of the index of geomagnetic activity Dst, the storms are usually classified as moderate (minimum Dst excursion above −100 nT), intense (minimum Dst lies between −250 nT and −100 nT), and super-storms (Dst below −250 nT). Besides extreme Dst variations, super-storms are often characterized by drastic long-term (>3 h) changes in the ionosphere, such as dayside ionospheric uplift and development of the dayside ionospheric super-fountain effect, when the dayside total electron content (TEC) within the crests of the equatorial ionization anomaly (EIA) can exceed ~25% the background levels and the EIA crests travel poleward for more than 10–15° of latitude from their regular position, spreading toward midlatitudes [e.g., *Tsurutani et al.*, 2004; *Mannucci et al.*, 2005; *Astafyeva et al.*, 2007; *Astafyeva*, 2009a, 2009b]. During less intense ionospheric storms, the maximum value of the dayside TEC does not exceed 60–80 TECU, and the EIA crests do not travel far from their "undisturbed" position of ±15° of magnetic latitude.

Intense ionospheric storms can have a crucial impact on the global navigational satellite systems (GNSS) that use radio signals reflecting from or propagating through the ionosphere. Large and rapid variations of electron density during ionospheric storms change the propagation velocity of radio waves, introducing a propagation delay, and cause fluctuations of phase and amplitude of GPS signals, also known as ionospheric scintillations, which may, eventually, result in cycle slips and losses of carrier lock. Such scintillations are known to be caused by irregularities with scale sizes of the order of the first Fresnel zone size [*Yeh and Liu*, 1982; *Pi et al.*, 1997]. At GPS frequencies (1.227 and 1.575 GHz), the horizontal scale of the first Fresnel zone equals to 150–300 m for irregularities at an altitude of ionospheric *E* and *F* regions [e.g., *Yeh and Liu*, 1982; *Pi et al.*, 1997; *Afraimovich et al.*, 2009].

Polar, auroral and equatorial regions are known as regions with irregular plasma distribution, especially under high geomagnetic activity. Contrary to high and low latitudes, the midlatitude ionosphere is generally regarded as a less irregular environment and, at L-band frequencies, is considered to be free of scintillations, lacking the necessary mechanisms commonly required to generate irregularities. However, during strong geomagnetic storms the auroral oval moves equatorward and the EIA expands toward midlatitudes, so that the midlatitude

Table 1. General Information About the Events (Date, Time of the Sudden Commencement, Minimum of the Bz and Symmetric Disturbance Field in H Component (SYM-H) Excursions, Maximum Value of the Dayside Total Electron Content (TEC), and Signatures of SFE) and Their Influence on GPS Performance (Density of LoL at L1 and L2 GPS Frequencies, and of TEC Slips)

Date	SSC, UT	Min IMF Bz	Min SYM-H	TECmax, TECU	SFE	LoL L1,%	LoL L2, %	TEC Slips, %
07/09/2002	16:37	−23 nT	−144 nT	150–180	+	0.15	2.1	2
20/11/2003	8:05	−51 nT	−422 nT	170–180	++	0.25	2.8	9.5
15/05/2005	5:40	−42 nT	−302 nT	70–80	?	0.19	1.4	3.5
24/08/2005	2:39	−55 nT	−220 nT	60–70	–	0.15	0.9	1

ionosphere becomes quite perturbed and irregular. For instance, during the main phase of geomagnetic storm of 25–26 September 2001, severe GPS L1 amplitude scintillations were observed for the first time in the midlatitude region [*Ledvina et al.*, 2002]. Midlatitude scintillations and numerous count omissions in GPS data were also observed during a series of geomagnetic storms in 2000–2003 [*Afraimovich et al.,* 2004, 2009]. The omissions were found to occur at the boundary of the auroral oval, which is known as a region with intense small-scale irregularities of electron density. *Demyanov et al.* [2012] showed other spectacular example of occurrence of GPS errors at midlatitudes: during a geomagnetic storm of 12 February 2000 with minimum Dst excursion of −133 nT a super bubble of plasma density was observed over Japan [*Ma and Maruyama*, 2006]. For the satellites with LOS close to the magnetic zenith region, the density of GPS Losses-of-Lock reached 32%. In addition to carrier-phase slips, the super-bubble caused sharp increases in positioning error at receiver locations below 38°N latitude.

Thus, there have been performed numerous studies on errors in GPS performance under geomagnetically disturbed conditions [*Skone and de Jong*, 2000, 2001; *Doherty et al.*, 2001; *Afraimovich et al.*, 2002, 2003, 2011; *Jakowski et al.,* 2005, 2007; *Basu et al.*, 2008; *Rama Rao et al.*, 2009; *Bergeot et al.*, 2011]. However, less attention seemed to be paid on dependence of these effects on a magnitude of ionospheric storm time changes, and on the global (latitudinal and longitudinal) distribution of GPS "errors." *Pi et al.* [1997] suggested monitoring the distribution of ionospheric irregularities using the worldwide GPS network. Based on the rate of TEC (ROT) parameter, they showed that GPS phase fluctuations became stronger at high latitudes during geomagnetic storm of 10 January 1997 (during minimum of solar activity). Similar results were later shown for other events, including super-storm of April 2000 and a storm of 9 March 2012 [*Pi et al.,* 2011, 2013].

In this work, we study global occurrence and distribution of GPS Losses-of-Lock (LoL) and TEC slips during four geomagnetic storms of different intensity that occurred in the 23rd solar cycle (Table 1). Our work opens an opportunity for the future possibility to forecast the quality of GPS performance in different regions of the Earth from the initial geophysical parameters at the beginning phase of geomagnetic storms.

For our analysis we used data of GPS receivers in RINEX format from global networks (e.g., IGS, UNAVCO, Sonel) as well as numerous regional networks (in New Zealand, Australia, North and South America, Asia, Africa as well as islands in the oceans), in order to obtain better global coverage and to better understand the effects of the space weather events in different longitudinal and latitudinal regions. The total number of stations used in our study is ~1100–1970 for each event (Figure 1).

2. GPS Losses-of-Lock and TEC Slips as Main Indicators of GPS Performance Quality

To study the effects of intense ionospheric storms on GPS-based navigation systems, we analyzed two main parameters:

1. Density of GPS Losses-of-Lock at both GPS frequencies L1 and L2, at each station and the global value. As a loss-of-lock, we consider absence of observations at L1 or L2 in the output RINEX file. First, we estimate the number of GPS LoL at each frequency at each GPS station. Second, we count the total number of possible measurements. Third, we calculate the relative density of GPS LoL at each frequency:

$$P_{1,2} = \frac{N_{1,2}}{S} * 100, \% \quad (1)$$

where $N_{1,2}$ is the number of LoL at L1 and L2, respectively, and S is the total number of measurements. To plot the maps of GPS LoL density, we perform such calculations for each station separately, and we calculate the global value by summing values from all receivers. We further estimate the contribution of

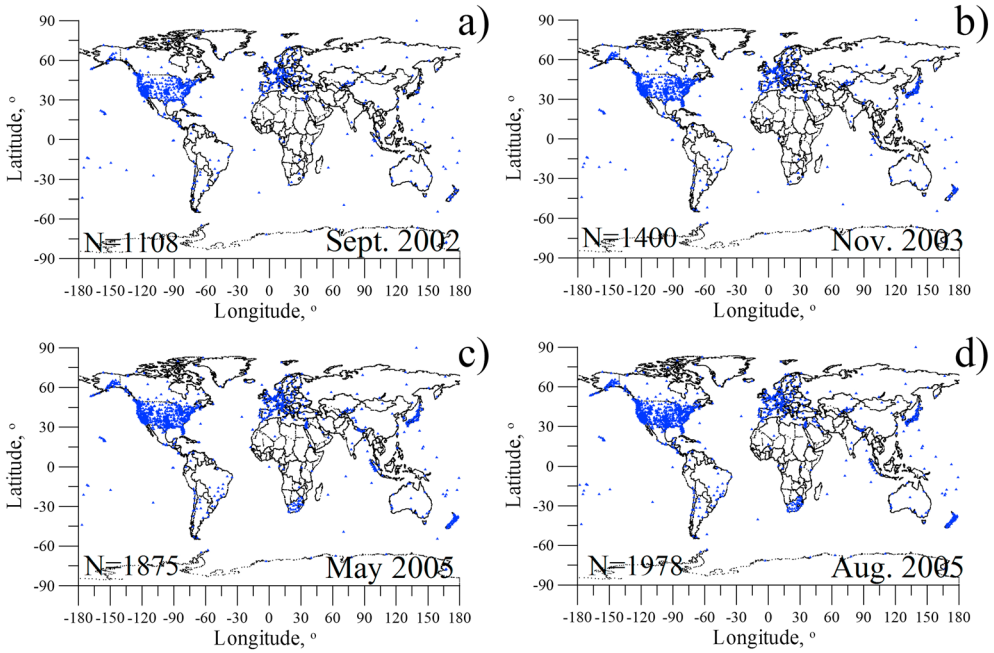

Figure 1. Map of GPS receivers used in the work for the storms: (a) 7 September 2002; (b) 20 November 2003; (c) 15 May 2005; and (d) 24 August 2005. The positions of the receivers are shown by blue triangles; the number N of GPS receivers is indicated in the bottom left corner of each panel.

the day- and nightsides in the total number. As a dayside, we consider a part of ionosphere lighted at an altitude of 200 km. For this purpose, we calculate the line of the solar terminator and choose the certain lines of sight. The day and night contributions were further divided by a total number of day and night observations, respectively, in order to obtain the ratios of LoL density. The cutoff of elevation angle is 10°.

2. Number of TEC slips that are calculated from deviations of TEC deduced from phase measurements. Here we suggest that a jump of slant TEC that we consider as a TEC slip depends on latitude, as the background value of TEC varies significantly with latitude. Thus, at equatorial and low latitudes (within ±25° of latitude) a TEC jump of 3 TECU per one 30 s interval in the RINEX file was counted as TEC slip. For the midlatitudes (between ±25° and ±75° Lat) and high latitudes (over ±75° of Lat) we consider a jump of TEC of 2 TECU/30 s and 1 TECU/30 s, respectively. The background value of TEC slips was estimated from the mean value of TEC slips on a reference day. The density of TEC slips is calculated in the similar way as the LoL, i.e., normalizing over the total number of measurements and multiplying by 100%.

Below we analyze the quality of GPS performance based on the value of these two parameters. The results are summarized in Table 1.

3. Geomagnetic Storms and Super-Storms and Occurrence of GPS Losses-of-Lock and TEC Slips

From 2000 to 2013, a large number of geomagnetic disturbances were recorded; however, only a dozen of events could be classified as super-storms, with occurrence of ionospheric super-fountain effect (SFE) and the consequent drastic TEC increase within the crests of the EIA. Some of these superstorms (6 April 2000, 15–16 July 2000, 30–31 March 2001, 5–6 November 2001, 17 April 2002, 29–31 October 2003, 20 November 2003, and 7–12 November 2004) and their effects on GPS-based navigation have been extensively discussed in scientific literature [e.g., *Afraimovich et al.*, 2002, 2004; *Kelley et al.*, 2003, 2010; *Tsurutani et al.*, 2004; *Astafyeva et al.*, 2007; *Foster and Coster*, 2007; *Mannucci et al.*, 2008, 2009, 2014; *Astafyeva,* 2009a, 2009b; *Basu et al.*, 2008; *Rama Rao et al.*, 2009; *Bergeot et al.*, 2011]. In this paper, we will perform comparative analysis of ionospheric effects on GPS performance during storms of different intensity: two super-storms—of 20 November 2003 and 15 May 2005 and two less intense geomagnetic storms—of 7 September 2002 and of 24 August 2005. The latter two could be classified as intense storms according to the values of symmetric disturbance field in

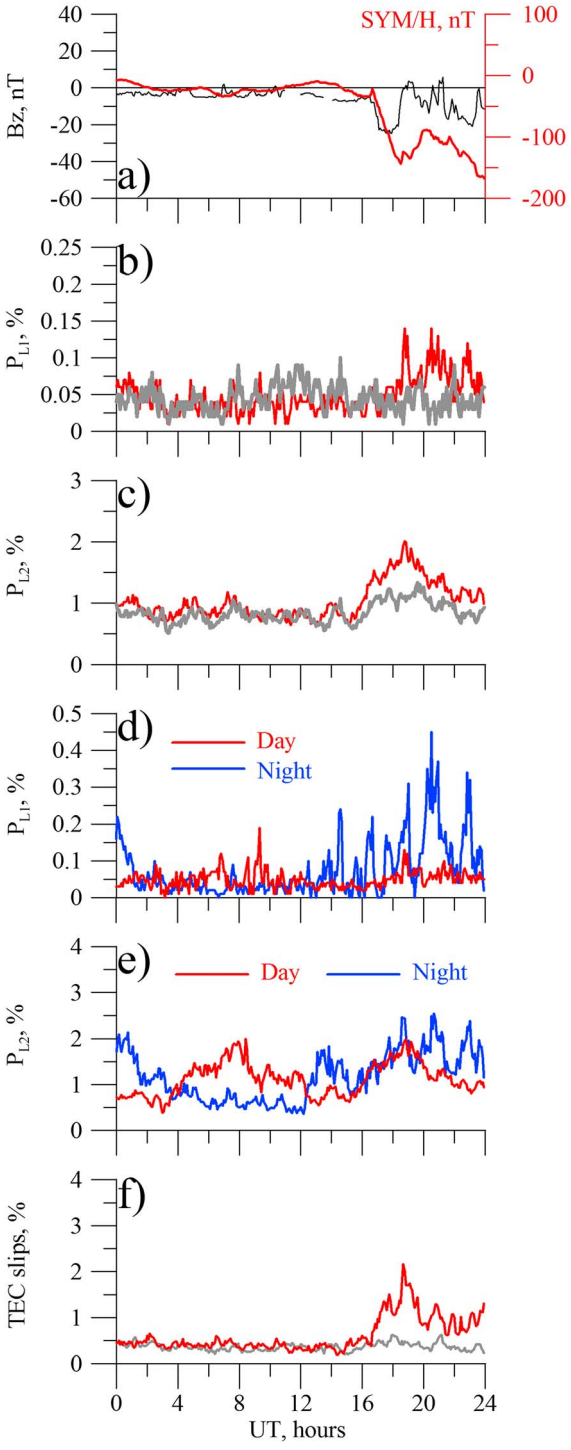

Figure 2. (a) Variations of the index of geomagnetic activity symmetric disturbance field in H component (SYM-H) (red) and of the interplanetary magnetic field (the Bz component, black curve) during the storm of 7 September 2002; (b) density of GPS Losses-of-Lock (LoL) at the main GPS frequency L1 for the day of the storm (red) and the reference day (gray); (c) density of GPS LoL at auxiliary frequency L2 on the day of the storm (red) and the reference day (gray); GPS LoL on the dayside (red) and nightside (blue) hemisphere at L1 (d) and L2 (e); and (f) global value of GPS total electron content (TEC) slips for the day of the storm (red) and the reference day (gray). The reference day is 3 September 2002.

H component (SYM-H) index (same as the 1 h Dst index but with 1 min resolution), but which did not cause significant changes in the ionosphere (Table 1 and Figures 4a and 5a).

3.1. Geomagnetic Storm of 7–8 September 2002

The storm of 7 September 2002 commenced at 16:37 UT by the abrupt decrease of Bz IMF from −7 nT to −23 nT within 15 min (Figure 2a). By 17:39 UT the Bz reached its minimum value of −26.11 nT, and it remained below −20 nT till 18:25 UT. At 18:50 UT the Bz reached 0 nT and varied around this value within the next hour. Such strong negative variations of the IMF Bz component caused a drop in the global storm index SYM-H from −29 nT at 16:48 UT to the minimum of −144 nT at 18:30 UT (Figure 2a). From 19:30 UT the SYM-H started to increase rapidly but at 20:30 UT it decreased again in response to the second drop of the IMF Bz. Overall, the main phase of the storm continued till ~1 UT of the next day.

Despite not being a super-storm, this event showed some signatures of the dayside SFE in data of satellite and ground-based instruments [*Astafyeva*, 2009a; *de Abreu et al.*, 2010]. Thus, around 19 UT satellite altimeter Jason-1 crossed the 13 LT sector and observed a storm time TEC value of 189 TECU in the northern EIA crest and 154 TECU in the southern one [*Astafyeva*, 2009a]. At the same time, the EIA trough value decreased to 60 TECU, and the distance between the crests increased to 50° of latitudes. All these signatures indicate on the enhancement of the fountain effect and development of the super-fountain effect along with dayside ionospheric uplift. The latter is also well seen in the data of the SAC-C satellite, with observations of TEC enhancement above 715 km of altitude at ~19 UT. Overall, the dayside storm time effects spread from the forenoon to late afternoon sectors and were observed during at least 2–3 h [*Astafyeva*, 2009a]. Apart from the satellite observations, ionospheric response to this storm was analyzed in details in the American sector by use of ground-based GPS receivers and digital ionosonde stations [*de Abreu et al.*, 2010]. A strong hemispheric asymmetry was observed in the ionospheric response, as the

TEC variations were observed to be less affected by the storm in the Southern American sector. Signatures of the positive ionospheric storm were observed in both hemispheres at midlatitude stations.

To analyze the impact of this ionospheric storm on GPS performance, we calculate the density of Losses-of-Lock at both main L1 and auxiliary L2 frequencies, as well as the density of TEC slips for the day of the storm 7 September 2002. We further compare the storm values with those of a quiet (reference) day of 3 September 2002 (gray curves in Figures 2b, 2c, and 2f). One can see that the background level of LoL does not exceed 0.05–0.08% for L1 GPS frequency and 0.8–1% for L2 LoL. The storm time values reach 0.15% and 2%, respectively, at the main phase of the geomagnetic storm from 16:30 to 19:30 UT (Figures 2b–2c). The contributions of the day and nightsides are shown in Figures 2d–2e). We see that during this storm, at L1 the nightside contribution to the total value of LoL density was much larger than that of the dayside. Several large peaks are seen from 14 to 24 UT, with maximum of 0.45% at ~20 UT (Figure 2d, blue curves). Whereas, the maximum of 0.2% of the dayside value was reached at ~9 UT (Figure 2d). The value of LoL density at the auxiliary frequency L2 seems to have less correlation with the storm development. We observe two small peaks of 2% in the dayside curve, at 9 UT (before the storm) and at 19–20 UT (during the storm), and 2–2.5% increases on the nightside at 13 UT, and at 17–20 UT (Figure 2e). The peaks in the nightside curve might be related to the post-sunset enhancement in the equatorial anomaly, as often observed during large ionospheric storms [e.g., *Basu et al.*, 2007].

The total value of the TEC slips during the day of the storm is shown in Figure 2f. One can see that the number of TEC slips starts to increase with the beginning of the storm at 16:50 UT and by 19:30 UT reaches its maximum value of ~2%, i.e., 4–5 times exceeding the background value. We observe overall a good correlation between the variations of the TEC slips number and that of the storm index SYM-H.

3.2. Geomagnetic Storm of 20 November 2003

The geomagnetic storm of 20 November 2003 was one of the most intense storms of the 23rd solar cycle and caused very significant and long-term changes in the ionosphere [e.g., *Basu et al.*, 2007; *Mannucci et al.*, 2008; *Zhao et al.*, 2008]. The storm sudden commencement (SSC) was registered at 8:03 UT on 20 November. The ionospheric disturbance started to develop after a sudden drop of the IMF Bz at 11:40 UT (Figure 3a). The IMF Bz further remained steadily southward during several hours, reaching its minimum of −52 nT by 15:50 UT. Consequently, the SYM-H index went down to −240 nT by 15:50 UT and continued to decrease within next few hours, till the minimum extreme excursion of −488 nT at 18:15 UT (Figure 3a). The IMF Bz returned to 0 nT by 1:30 UT of the next day, and the SYM-H index remained below −100 nT till 17:30 UT of 21 November.

Such long-term negative Bz event provoked a very intense ionospheric superstorm with TEC maximum level of 160 TECU in the noon and evening sectors and 170–180 TECU in the afternoon sector [*Mannucci et al.*, 2008; *Astafyeva*, 2009a]. The EIA crests moved away from the magnetic equator by 10° of latitude from their quiet position. Intense dayside ionospheric uplift was observed in satellite data for at least 2–3 h during this storm [*Basu et al.*, 2007; *Astafyeva*, 2009a].

Following such strong and long-term geomagnetic and ionospheric disturbance, the performance of the GPS was perturbed for several hours. The density of LoL at the main GPS frequency started to increase at ~17:30 UT, reached maximum of 0.25% at 20 UT, and decreased to background level by 23 UT (Figure 3b). The density of LoL at L2 frequency started to grow around 15 UT, and it remained enhanced till 22 UT (Figure 3c). The maximum value of ~3% was reached by 18:30–19 UT. Figure 3d shows that the bulk contribution to the global value of the L1 LoL was made by the stations situated on the nightside; it is contrary to the L2 LoL, where both day and nightside parts seemed to contribute equally in the total value during the main phase of the super-storm (Figure 3e).

The global number of the TEC slips started to increase slightly from 14:30 UT, and from 18 UT it rapidly increased till 9.5% by 19:30 UT, which gives almost 40 times increase over the background (~0.25%). By 23 UT it decreased till undisturbed level (Figure 3f).

As in the case of the previous example of the storm of 7 September 2002, we remark a good correlation with variations of SYM-H index. Besides, during this storm, all the parameters indicate simultaneously on perturbation.

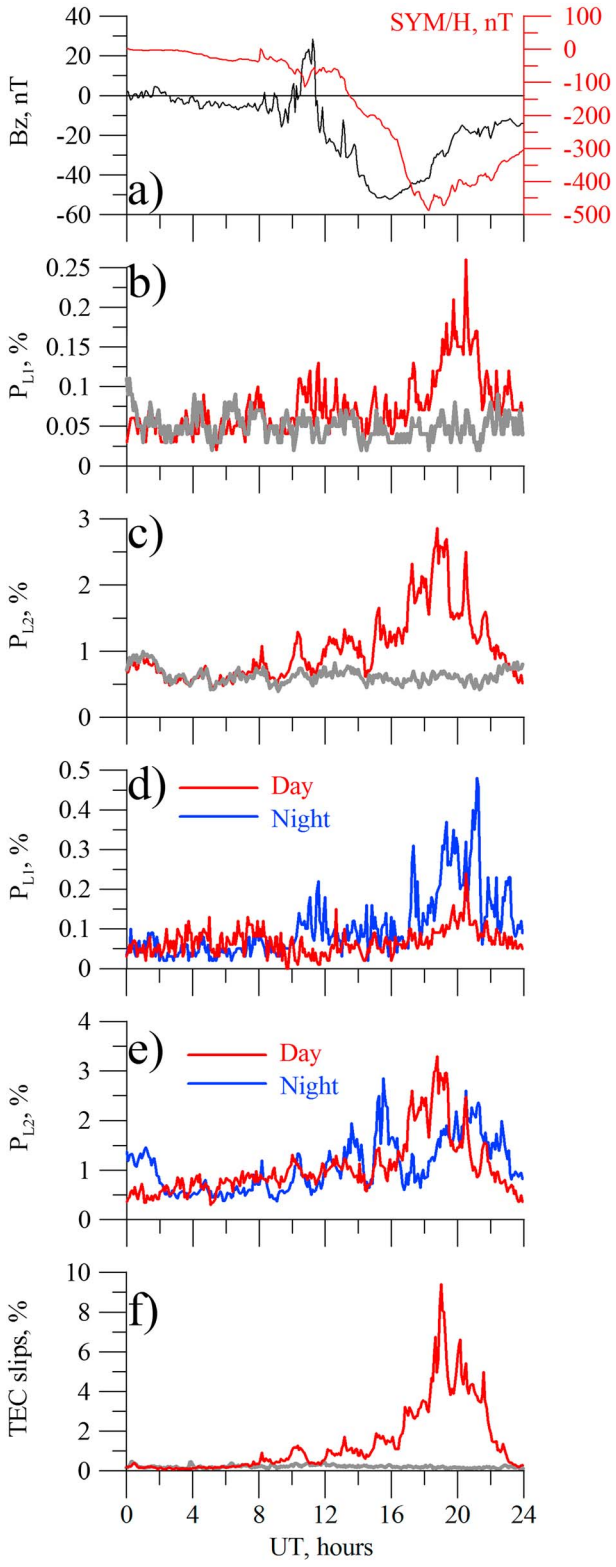

Figure 3. Same as Figure 2 but for the super-storm of 20 November 2003 and a reference day 19 November 2003.

3.3. Geomagnetic Storm of 15 May 2005

The storm sudden commencement was recorded at 2:40 UT with a sudden increase of the interplanetary plasma flow speed (not shown) and a sharp increase of the SYM-H (Figure 4a). However, the ionospheric storm began to develop around 06 UT, when the IMF Bz dropped suddenly from +36 nT to −42 nT (Figure 4a). The IMF Bz remained negative for the next 3 h and turned northward at 9 UT. Such IMF Bz negative event provoked an intense geomagnetic storm with the decrease of the SYM-H index down to the minimum value of −302 nT by 8:20 UT. The SYM-H further remained below −200 nT till 9:50 UT and below −100 nT till around 21 UT.

Observations made in Brazilian [*de Abreu et al.*, 2011] and in Indian equatorial and low-latitude sectors [*Dashora et al.*, 2009] by use of ground-based GPS measurements and data of ionosondes reported on signatures of a large positive ionospheric storm shortly after the SSC at 02:39 UT. The vertical TEC observations indicated a strengthening of the nighttime EIA in the Brazilian region [*de Abreu et al.*, 2011], a dayside uplifting of the *F* region and an overall enhancement of the dayside equatorial fountain effect in the Indian region [*Dashora et al.*, 2009; *Ngwira et al.*, 2012] and over South Africa [*Ngwira et al.*, 2012]. The presence of convection electric fields was observed based on data of ground-based magnetometers [*Dashora et al.*, 2009; *Ngwira et al.*, 2012]. According to our knowledge, no signatures of the SFE have been reported as from satellites observations, as in the case of two previously described events.

The impact of the storm of 15 May 2005 can be concluded from Figures 4b–4f. The density of LoL at the main GPS frequency sharply increased to 0.2% at ~6:30 UT, i.e., during the development of the ionospheric storm (Figure 4b). The density of LoL at L2 grew up to ~1.5% at 6:10 UT and remained 3 times more than the background level till ~8:50 UT (Figure 4c). At L1, the main contribution to the storm time global value of LoL was made by the dayside GPS receivers (as seen from Figure 4d), whereas at L2, apart from the contribution by the dayside,

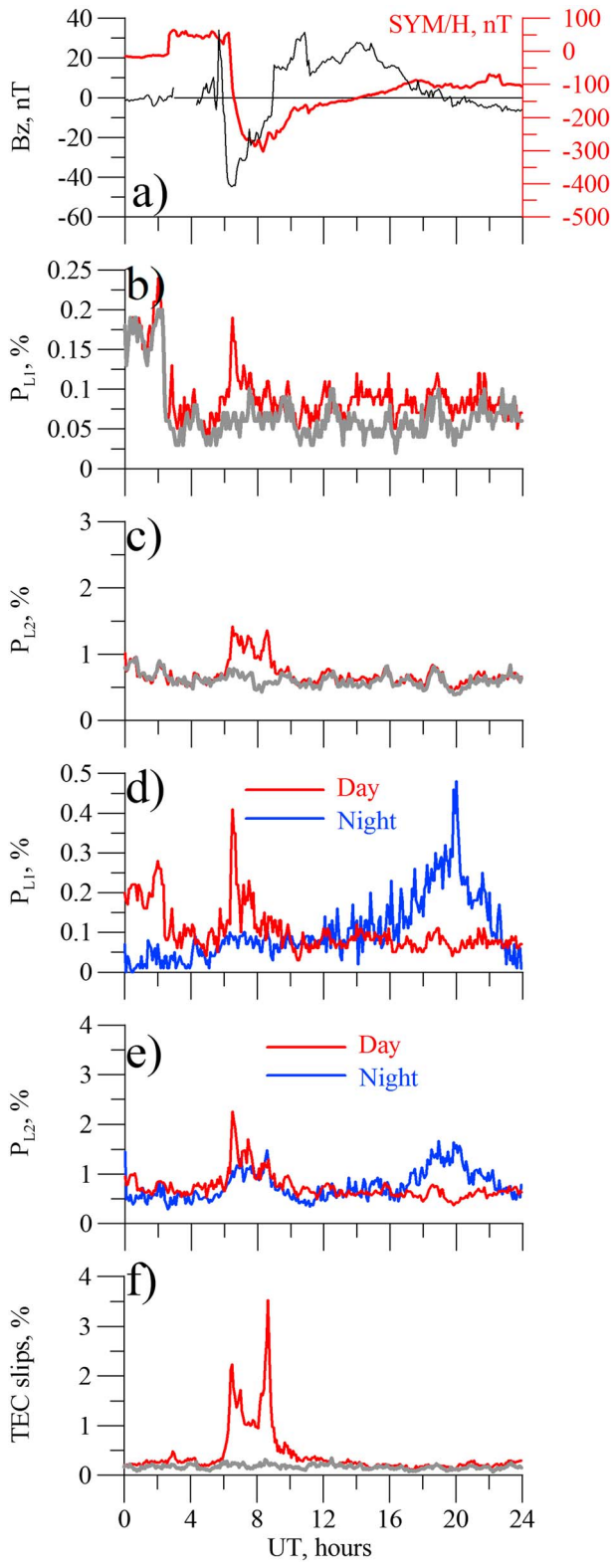

Figure 4. Same as Figure 2 but for the super-storm of 15 May 2005 and a reference day 14 May 2005.

we also observe a small nightside increase of the ratio of GPS LoL at the main phase of the geomagnetic storm of 15 May 2005 (Figure 4e). Note that we observe an essential increase of the nightside LoL ratio at ~18–22 UT at L1 frequency and a small peak at L2 frequency at 19–20 UT, i.e., at the recovery phase (blue curves in Figures 4d–4e). This finding is similar to that for the storms of September 2002 and November 2003; however, for the two previous storms the nightside peak corresponded to the main phase of the storms, while in the case of the May 2005 storm there seems no correlation between the storm activity and the increase of the LoL L1 density on the nightside of the Earth. Also, we see a large peak of the global L1 LoL density that occurred from 0 to ~2 UT, on both the storm day and also on the reference day, whose intensity is as large as that during the storm (Figure 4b). Analysis of the day and night contributions indicates that these peaks were caused by some effect of the dayside (as seen from Figure 4d). More detailed analysis of these findings will be done in section 4.

The global number of the TEC slips showed two maxima, first smaller peak of 2.3% was registered at ~6:20 UT (coincides with the time of the LoL L1 increase) and the second larger peak of 3.5% appeared at ~8:30 UT. These peaks exceed considerably the background and undisturbed value of TEC slips (Figure 4f). We point out on an overall good correlation of sudden quasi-simultaneous change of all parameters in Figure 4. However, unlike for the previous two storms, in the case of May 2005 storm, we find that the density of LoL as well as the ratio of TEC slips starts to increase shortly before the drop of the SYM-H index.

3.4. Geomagnetic Storm of 24 August 2005

The commencement of the storm was recorded at 6:13 UT, when the SYM-H index rapidly increased from 10 to 30 nT (Figure 5a). The largest ionospheric changes occurred shortly after the sudden drop of the IMF Bz at 9:10 UT, which reached its minimum of −55 nT by 10 UT. The SYM-H index began to decrease at 10 UT and the minimum excursion of −173 nT was reached by 11:10 UT. Despite such large variations of interplanetary and

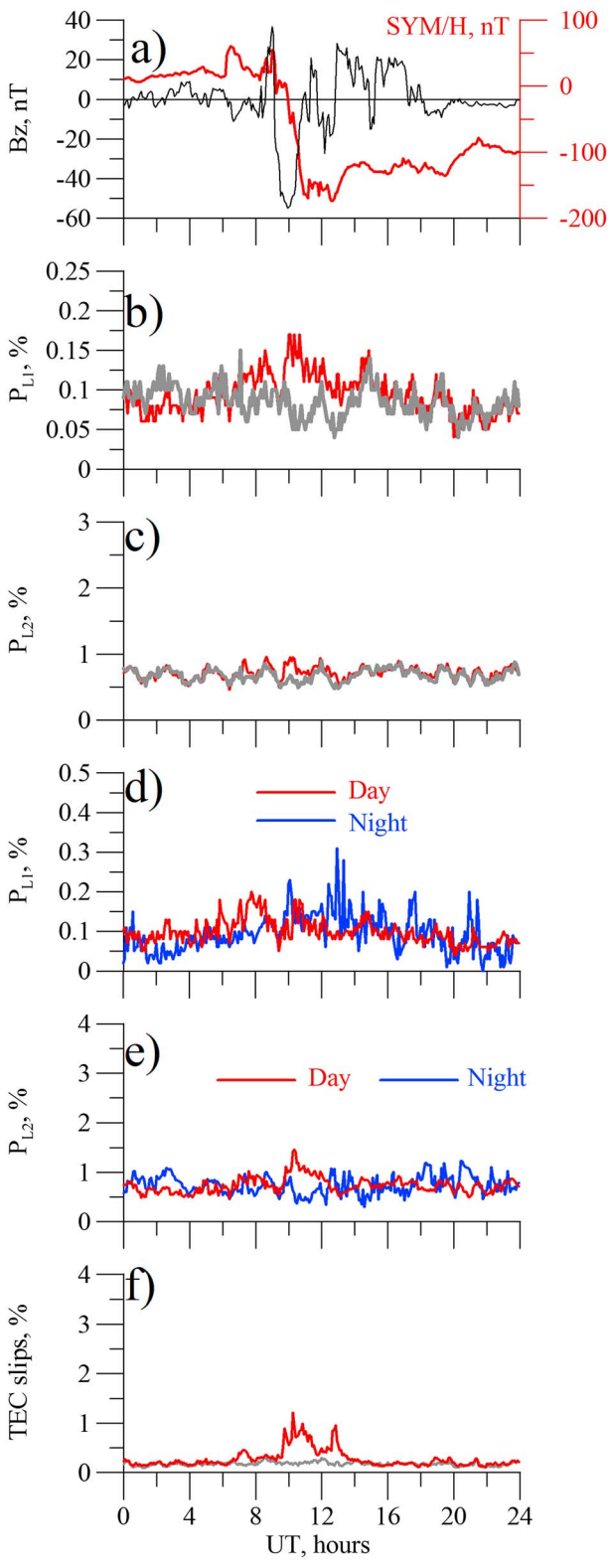

Figure 5. Same as Figure 2 but for the storm of 24 August 2005 and a reference day 23 August 2005.

geophysical parameters, and contrary to super-storms, no signatures of the dayside super-fountain effect were observed in satellite data during this storm [*Astafyeva*, 2009b]. Measurements from CHAMP satellite that passed in the evening sector (~19:30 LT), showed that during the main phase of the storm the maximum dayside TEC level reached 60–70 TECU within the crests of the EIA, whereas the quiet time TEC did not exceed 30 TECU. Ground-based observations in the Brazilian, American, and European regions indicated on observations of prompt penetration of magnetospheric electric fields and on occurrence of signatures of positive ionospheric storms in these regions [*Paznukhov et al.*, 2009; *de Jesus et al.*, 2012].

According to our analysis, the storm of 24 August 2005 did not cause a strong impact on the quality of GPS performance, as the curves of LoL density at both frequencies show the lowest levels out of four storms under consideration (Figures 5b–5e). Thus, the density of LoL at the primary GPS frequency hardly exceeds the background level of LoL calculated for the reference day 23 August 2005 (Figure 5b), reaching ~0.157% during the main phase of the storm; the curve of the L2 LoL density does not go beyond the background value (Figure 5c). At L1 frequency, slightly larger contribution to the storm time value of LoL density seems to be made by the nightside GPS receivers (a small peak of 0.2–0.3% around ~10–13 UT) (Figure 5d). At L2 frequency, we see a little larger contribution from the dayside GPS receivers, though that it is only 0.5% larger than the background value of L2 LoL (red curve in Figure 5e).

At the same time, the global ratio of TEC slips calculated for the whole day of 24 August 2005 clearly shows the period of the ionospheric perturbation from ~8:50 UT to 13 UT. The maximum number of 1.4% (i.e., almost 6 times over the background level) of the TEC slips is reached by 10 UT, and another small peak is seen at ~12:30 UT, which coincides with the time of the minimum of the IMF Bz component and to the time of the sudden drop of the index SYM-H (Figure 5f).

4. Global Distribution of GPS Losses-of-Lock and TEC Slips. Regions With Largest Contribution to the Global Values

Previously, we have shown variations of the global number of the density of GPS LoL at both GPS frequencies, as well as the density of TEC slips on the day of ionospheric storms and super-storms under consideration. The largest effects were observed during the event of 20 November 2003 and of 15 May 2005, which were earlier classified as super-storms. As for the other two events, though that the storm time ionospheric effects were sufficiently large, the storms of September 2002 and of August 2005 did not show very significant impact on the operational quality of GPS receivers. In all the cases, the period of storm time perturbations can be clearly seen in the curves, either in TEC slips (7 September 2002 and 24 August 2005) or in both LoL and TEC slips (events of 20 November 2003 and 15 May 2005). Then, except for the storm of 24 August 2005, we clearly observe a large peak of the nightside L1 LoL around 19–20 UT. It is important to note that for the storms of September 2002 and November 2003 the nightside peak falls onto the main phase of the storm, which explains the increase of density of L1 LoL during evening hours, as the post-sunset sector is often characterized as irregular. Whereas, in the case of the May 2005 event the large increase of L1 LoL occurs at the recovery phase, so that such increase of GPS slips is somewhat unexpected. This observation makes us suggest that the found nightside effect was not related to the storm but was provoked by some other background phenomenon. Another curious finding was a large peak in the LoL global density at L1 frequency before the beginning of the storm of 15 May 2005, the nature of which is not clear from the global curves. To clarify these issues and to better understand regional contributions in the global value, we make global maps of density of GPS LoL (upper and middle panels) and of TEC slips (bottom panel) as shown in Figure 6 on the example of the 20 November 2003 super-storm. One can see that at 18:58 UT (18.871 UT in Figure 6) the quality of GPS performance at the principal GPS frequency worsened at high latitudes of the northern hemisphere. At the same time, numerous L2 LoL occurred in practically all latitudinal regions on the sunlit side (American and Pacific sectors, including the morning midlatitude sector around New Zealand). We also observe an increase of rate of GPS LoL density in the post-sunset sector (over Europe). The most spectacular effects were observed for TEC slips over North Europe and over almost entire North America, largely including midlatitudes. In southern hemisphere, the GPS coverage was less dense, but we could notice storm time effects over Antarctica and also around South Australia and New Zealand. We find that in southern hemisphere the TEC slips also reach midlatitudes (till ~40°S). Thus, such global map of TEC slips provides a direct indication on distribution of intense ionospheric irregularities.

To trace the evolution of global distribution of GPS LoL density at both frequencies as well as of TEC slips during the storm days, here we present Animations 1 and 2 (available as supporting information). Due to the lack of space, we only show the maps for the storms of 20 November 2003 (Animation 1) and of 15 May 2005 (Animation 2). For both events, occurrence of LoL at L1 frequency is very low in general, while the auxiliary frequency L2 appears to be much "noisier," showing numerous LoL even during quiet conditions. The latter is, most likely, because of less power strength of L2 GPS signals [e.g., *Afraimovich et al.*, 2008]. Largest storm time effects on GPS performance at L1 frequency can be seen during the maximum ionospheric disturbance on 20 November 2003, i.e., from 17:00 to 21:30 UT, in American and especially in the European regions (Animation 1, upper panel). The latter from ~18 UT was on the nightside, which may explain the increase of the value of global LoL L1 from 18 UT in Figure 3.

As for the L2, several LoL can be seen global-wide throughout the day (Animation 1, middle panel); however, from 17:30 UT the LoL density significantly increases, especially in North American and European regions. This disturbance effect lasts till ~22:50 UT.

Contrary to the LoL, the TEC slips (Animation 1, bottom panel) occur occasionally global-wide only before ~7:40 UT, when the geomagnetic conditions were quiet. With the arrival of the interplanetary shock at ~8 UT (the SSC time), we observe occurrence of many TEC slips at high latitudes in both north and south hemispheres. This effect lasts till ~10:40 UT. From ~12 UT, TEC slips occur more intensely in the auroral regions, and the regions of TEC slips expand till ~45–50°N as can be seen in regions with dense coverage. From 16:30 UT a new very strong "wave" of a large number of TEC slips can be seen in all sectors, and especially over North of North America and over Northern Europe, where the area of perturbations descends more toward midlatitudes (below 40°N). By 18:30 UT, we observe further descent of the perturbation to below 25°N in the American and African–European sectors and till −40°S around New Zealand. At some GPS stations, the level of TEC slips reaches 60–70%. From 21:40 UT the perturbation area starts to move back toward high latitudes and by 22:30 UT it clears off from TEC slips.

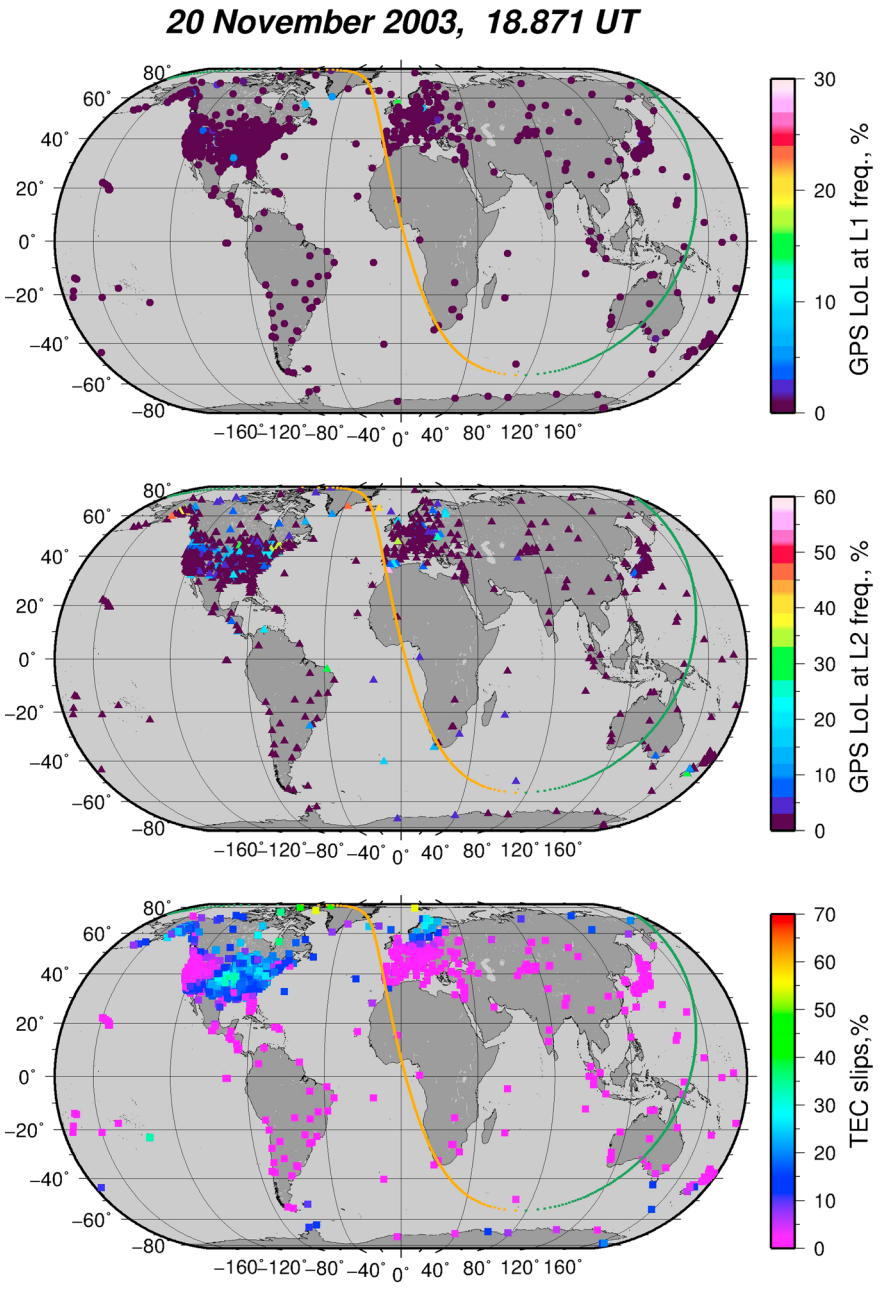

Figure 6. Global maps of density of GPS LoL at L1 and L2 frequencies (top and middle panels, respectively) and of TEC slips (the bottom panel) during the main phase of the super-storm of 20 November 2003 (at 18:50 UT). All parameters are 10 min averaged. Green and orange lines indicate the positions of the sunrise and sunset solar terminators, respectively, at height of 200 km.

On 15 May 2005 several strong L1 slips occur before the beginning of the storm on the dayside (Animation 2, upper panel). Apparently, GPS stations located in Northern Europe and in Australian region have sufficiently large number L1 LoL to influence the global as well as the dayside curves of the LoL density as seen in Figures 4b and 4e. At the time of the SSC at 2:40 UT more L1 slips were registered in northern and southern high-latitude regions; this effect continued till ~8:30 UT.

One of the largest questions opened in section 3.3 was on the large ~0.5% peak in L1 slips on the nightside hemisphere at the recovery stage of the storm of 15 May 2005 (Figures 4b and 4e). Detailed analysis of the global maps of LoL at L1 frequency shows up to 20–25% of slips at station YIBL (22.18°N; 56.11°E) from

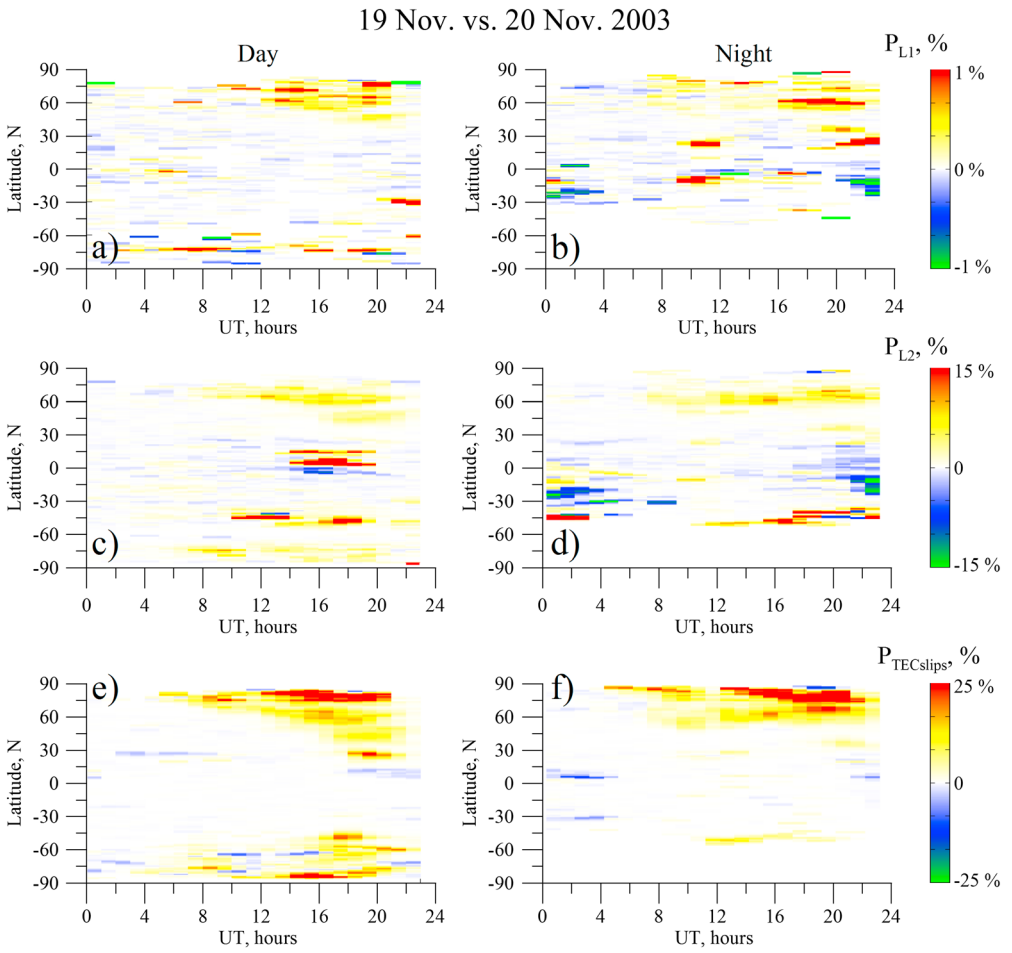

Figure 7. Latitudinal-temporal distribution of the density of LoL (a, b) at the principal GPS frequency L1, (c, d) at auxiliary GPS frequency L2 (e, f) and of TEC slips calculated for the case of the super-storm of 20 November 2003 and the reference day 19 November 2003: Figures 7a, 7c, and 7e are for dayside, and Figures 7b, 7d, and 7f are for nightside.

~17:30 UT to ~22:30 UT (upper panel). We consider that such high values of slips recorded at one single station together with sufficiently low number of the total nightside observations is the reason of the peak that appeared in Figure 4b. This observation suggests the importance of global maps of GPS slips.

The majority of L2 slips occurred between 2:40 UT and 11 UT at middle and high latitudes (middle panel of Animation 2). During this storm, occurrence of LoL starts at the time of SSC and continues throughout the main phase. In similar way, at the time of SSC at 2:40 UT, we observe first occurrence of TEC slips at high latitudes that lasts till ~3:20 UT (lower panel). Further, a large number of TEC slips was registered from ~6 UT with the development of the main phase of the storm. Maximum perturbation was reached by 8:00–8:30 UT, when we observed a large area with TEC slips over North America (nightside). From ~9 UT the level of TEC slips returned to quiet time level.

To have a single picture with latitudinal regions of the largest contribution to the global values of slips, we plot global reference maps for LoL and TEC slips for the day of the super-storm of 20 November 2003 and for the day of the storm of 15 May 2005, as compared to previous quiet days 19 November 2003 and 14 May 2005, respectively. To obtain such maps, we first analyze occurrence of LoL and TEC slips at each existing sub-ionospheric observational point. We then accumulate for 1 h the number of slips with a step of 1° of latitude. Once such calculations are made for these 2 days, we subtract the quiet day map from the storm day one; then positive values would mean occurrence of GPS LoL due to a storm, whereas negative difference between the two signifies lesser number of LoL at a particular place as compared to the quiet day, which is due to the displacements of ionospheric irregular structures during storms.

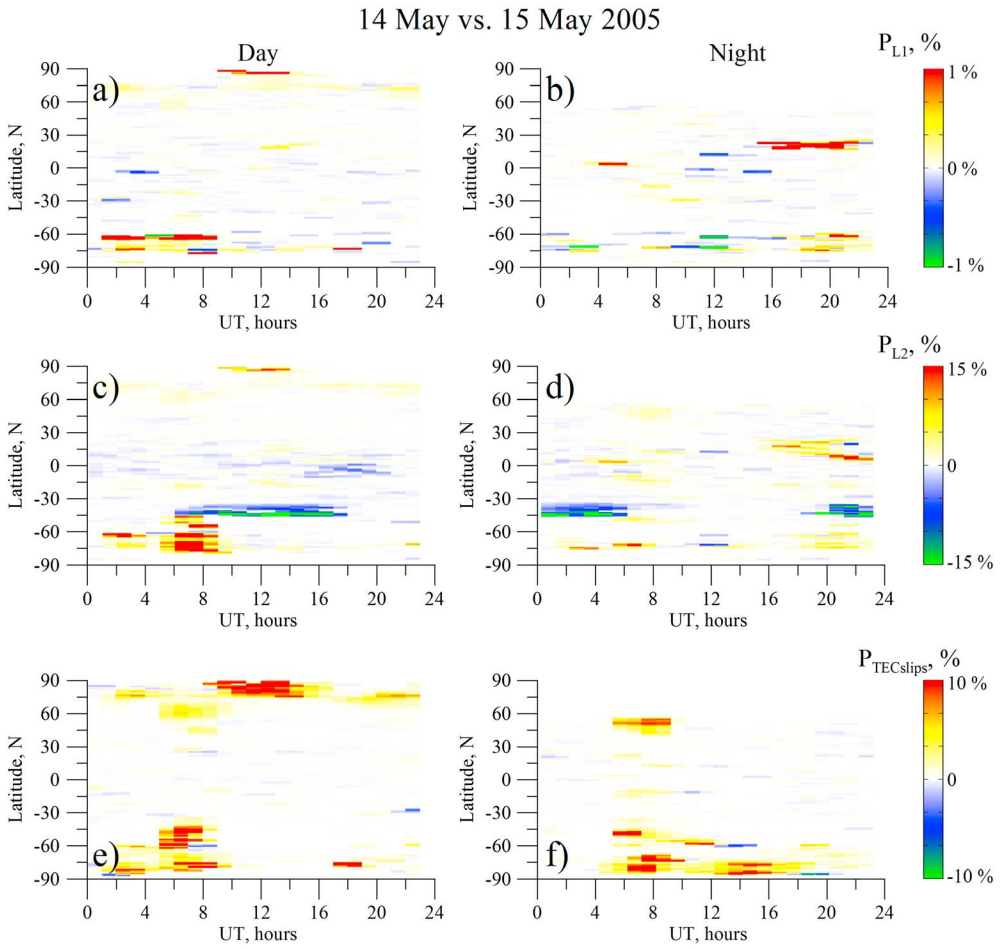

Figure 8. Same as Figure 7 but for the storm of 15 May 2005 and reference day 14 May 2005.

The results of our calculations for the day- and nightsides for the events of November 2003 and May 2005 are shown in Figures 7 and 8, respectively. One can see that on the dayside storm time LoL at L1 frequence occur mainly from 12–13 UT till 21–22 UT in the area between 45 and 80°N (Figure 7a), which coincides with the period of the main phase of the super-storm of 20 November 2003. On the nightside, we see too small positive spots in the low-latitude region from 9 to 12 UT in both northern and southern hemispheres, as well as from 20 to 23 UT in the northern hemisphere. We also note occurrence of negative spots in the low-latitude region of the southern hemisphere from 0 to 4 UT, and also from 20 to 23 UT (Figure 7b). The negative values are also seen at the equator at 11–14 UT. These negative values indicate less perturbed regions as compared to the quiet day.

LoL at L2 frequency begin to appear at high latitudes on the dayside from 8 UT and remain till ~22 UT (Figure 7c). With the beginning of the storm, i.e., from 10 to 12 UT, we observe occurrence of LoL at middle and low latitudes; this effect lasts till 20 UT, i.e., it is observed during the minimum of SYM-H excursion. One can also see the negative difference (~−7%) at the equator at 14–20 UT (Figure 7d). On the nightside, the storm time effects are not so clear as on the dayside. For instance, we see both positive and negative differences before the beginning of the storm, between 0 and 4 UT. A clearer storm signature is observed at high latitudes of the northern hemisphere (from 8 to 23 UT, in the same manner as on the dayside). We also notice large storm time effect at midlatitudes in the southern hemisphere from 12 to 23 UT (Figure 7b). By the end of the day, at 19–23 UT we observe a negative differential effect at low latitudes, which may or may not be related to the storm, as we observe similar effect before the storm onset as well. Finally, the reference maps for TEC slips density show much clearer storm time effects on both dayside (Figure 7e) and nightside (Figure 7f). On the dayside, TEC slips start to occur at high latitudes before the main phase of the storm, at 4 UT, and this effect further largely develops from 8 UT, with the shock arrival. From 12 UT the area of the storm time TEC slips expands toward

midlatitudes and descending below 30°N in the northern hemisphere, and the dayside level of TEC slips at high latitudes reaches 25% as compared to the previous day (Figure 7e). On the nightside, the situation is quite similar for the northern high latitudes whereas no significant changes can be seen in the southern hemisphere (Figure 7f).

In the case of the event of 15 May 2005, storm time effects seem to be more pronounced in the southern hemisphere than in the northern one (Figure 8). The reference maps for the dayside LoL L1 show ~1% increase from 1 to 9 UT at high latitudes, and a small area of increased LoL L1 can be seen in the northern polar region from 9 to 14 UT (Figure 8a). Nightside maps show a small positive storm time changes in the equatorial region from 3 to 6 UT; besides, we also notice an increase of L1 LoL at 30°N from 16 to 23 UT (Figure 8b). This corresponds to the peak on the nightside of the global curve in Figure 4e. As we mentioned before, this effect seemed to be caused by a single station YIBL located in Oman. Besides this, we also notice a positive effect at high latitudes from 18 to 23 UT in the southern hemisphere, which might have "reinforced" the level of LoL on the nightside as shown in Figure 4e and which was not quite obvious from the global maps.

For the L2 LoL, we observe the strongest dayside relative enhancement on the dayside from 4:30 to 8:30 UT, i.e., during the main phase of the storm, at high latitudes in the southern hemisphere (Figures 8c and 8d). There is also a small dayside negative midlatitude deviation that starts during the storm (at 6 UT) and continues till 18 UT; it also occurs in the southern hemisphere. On the nightside, on the contrary, we do not observe visible effects during the time of the storm. In the meantime, we see midlatitude negative deviation before the storm as well as from 20 to 24 UT. Over all, the dayside changes of LoL number in the equatorial and low-latitudes regions are caused by the storm time redistribution of the EIA, which includes expansion of the EIA toward midlatitudes with concurrent TEC increase in the EIA crests and the TEC decrease over the magnetic equator. The high-latitude differential increase, most likely, corresponds to storm time expansion of the area of the auroral oval toward midlatitudes. Therefore, the differential maps of density of GPS LoL show storm time redistribution of ionospheric plasma and, especially, occurrence of intensive ionospheric irregularities at all latitudinal regions. Storm time effects on the density of TEC slips can be seen in both day and night hemispheres (Figures 8e–8f). On the dayside, we observe occurrence of TEC slips from 2 UT at high-latitude regions in both northern and southern hemispheres (Figure 8e). From 4 UT, the areas of ionospheric irregularities descend till ~30° of latitude and clear off by 9 UT. However, from 9 UT till 15 UT a 10% increase can be seen in the north polar region on the dayside (Figure 8e). On the nightside, we can see storm time increase of TEC slips number at 45°N –60°N and at 45°S–90°S, and in southern hemisphere this effect lasts till ~18 UT (Figure 8f).

5. Discussions and Conclusions

Using data of ~1100–1900 GPS receivers, we investigated the quality of GPS performance based on analysis of variations of the GPS LoL density and of TEC slips during four geomagnetic storms of different intensity that occurred during the 23rd solar cycle. In addition to the total values, we also plot the global maps and reference maps of GPS LoL and TEC slips in order to estimate the contribution of different regions into this global value.

The global background level of GPS LoL is sufficiently low, generally around 0.05% for the main GPS frequency L1 and 0.75% for the auxiliary frequency L2. We show that the level of GPS LoL increases at the main phase of geomagnetic storms, usually during the sudden drop of the index of geomagnetic activity SYM-H, and returns to the undisturbed level at the beginning of the recovery phase of a storm. The maximum density of GPS LoL increases with the intensity of the storm. Thus, during the events classified as ionospheric super-storms, the ratio of GPS LoL increases up to 0.25% and the main GPS frequency L1 and up to 3% at L2 frequency, at both frequencies, the storm time value 4–5 times exceeded the quiet time background level. During less intense geomagnetic storms, the global density of GPS LoL reaches 0.15% at L1 frequency and 1.0–1.5% at L2, which is 2–2.5 times higher than the background ratios. Similar results were obtained for the density of TEC slips. Specifically, we observe a good temporal correlation between the global number of TEC slips and the development of an ionospheric storm (Table 1). Dependence on the intensity of a storm is also correct for the TEC slips, i.e., generally we can expect more TEC slips during stronger storms. In addition, besides the geomagnetic storms, quiet time auroral activity can cause increase of LoL rate, and, in particular conditions, even a singular GPS station can largely contribute in the global rate of GPS LoL.

Overall, our results are in good agreement with previous studies. For instance, *Afraimovich et al.* [2002] analyzed occurrence of GPS phase slips during geomagnetic storms of 6 April 2000 and 15 July 2000 (both are super-storms

in our classification) and found that the relative density of phase slips at midlatitudes during the main phase of geomagnetic disturbances reached 0.4%, i.e., was 1–2 orders of magnitude more than that of geomagnetically quiet days. The results of *Afraimovich et al.* [2002] were calculated over a particular region of interest (e.g., North America or Europe) and were averaged over 2.3 h, whereas in the current work we calculate the global value of GPS LoL for each 30 s epoch. *Afraimovich et al.* [2002] also showed that the rate of GPS phase slips may depend on the brand of a receiver: thus, among GPS receivers ASHTECH, Trimble, and AOA, the most storm sensitive is AOA, while ASHTECH showed the best operational "resistance" under geomagnetically disturbed conditions. In our study, we do not take into account the brand of a receiver, considering quasi-even coverage by receivers of different brands.

Our global maps of GPS LoL and TEC slips give important information about the most perturbed regions during geomagnetic storms. In addition, reference maps with latitudinal-temporal distribution can be very useful. It was previously shown that GPS cycle slips mostly occur at auroral latitudes [e.g., *Skone and de Jong*, 2000], in low-latitude region [e.g., *de Paula et al.*, 2003; *Rama Rao et al.*, 2009], and even at midlatitudes during geomagnetic storms [e.g., *Ledvina et al.*, 2002; *Afraimovich et al.*, 2004, 2009]. Our present results demonstrate that, over all, global maps of GPS LoL reflect very well storm time redistribution of the ionosphere, with strongest effects at high and equatorial latitudes. Meanwhile, global maps of TEC slips appear mostly at high latitudes. We note that at some moments of time the area of numerous TEC slips represents a sort of a "belt" of several degrees of latitude and extended for several tens of degrees of longitude. Such belt was observed to move equatorward during the main phase of geomagnetic storms. This perturbation is, obviously, due to the enhanced auroral activity and may correlate with the storm time expansion of the auroral oval, whose boundary is characterized as a region of intensive small-scale ionospheric irregularities (and in our classification TEC slips at high latitudes are TEC gradients with rate of TEC change higher than 1 TECU/30 s). To check the latter carefully, we compare our maps of TEC slips with maps of auroral energy input as obtained from OVATION database (http://sd-www.jhuapl.edu/Aurora/ovation/) (Figures 9 and 10). We note on a good agreement between the position of the auroral oval and the distribution of TEC slips at the initial stage of the 20 November 2003 super-storm, at ~10:15 UT (Figure 9a). Similar conclusions can be done while comparing images at the time of minimum excursion of the IMF Bz and of maximum development of ionospheric storm, at 16:15 UT (Figure 8b). Unfortunately, no data of auroral oval positions were available for the period from 16:30 UT to 20:15 UT, which corresponds to the main phase of the November 2003 super-storm. At ~20:45 UT, we observe the auroral oval boundary at ~60°N over Europe and around 52° over North America (right panel in Figure 9b). These borders can also be seen from the map of TEC slips for all longitudes with exception of the region between 60°W and 90°W, where the area of numerous TEC slips descended below 40°N (Figure 9c, and also Figure 6 and Animation 1). This may mean that the auroral oval was more expanded toward midlatitudes than it is shown on the image Figure 9c. Otherwise, and more likely, such disagreement can be explained by other source of TEC slips than the boundary of the auroral oval, such as dayside storm-induced "plume" of enhanced electron density as was shown previously for some storm events [e.g., *Foster and Rideout*, 2005], or large-scale traveling ionospheric disturbances (TID) [e.g., *Astafyeva et al.*, 2008; *Nishioka et al.*, 2009].

For the event of 15 May 2005, we also find the correspondence of TEC slips areas with the boundary of the auroral oval, both at the initial stage of the storm at 02:45 UT (Figure 10a) and at the main phase at 06:00 UT (Figure 10b). Further, during the maximum development of ionospheric storm, at 08:15 UT, we clearly see the belt of TEC slips above North America at ~42–50°N, which coincides with the thin structure of the auroral oval (Figure 10c).

Thus, the global maps of TEC slips serve as a good indicator of occurrence of small-scale intense ionospheric irregularities, similar to ROTI maps by *Pi et al.* [1997, 2002, 2011, 2013], and, as shown here, TEC slips maps can also mark the storm time position of the auroral oval. Similarly, the global maps of GPS Losses-of-Lock reflect the ionospheric plasma redistribution, besides direct indications on regions where the quality of GPS performance degrades. With the development of the global network of GPS receivers, especially in the southern hemisphere, some other possibilities can be opened for monitoring of global activity of ionospheric density distribution. For instance, forecasting of GPS performance in different regions of the Earth from the initial geophysical parameters at the beginning phase of geomagnetic storms could be possible from data of ground-based GPS receivers.

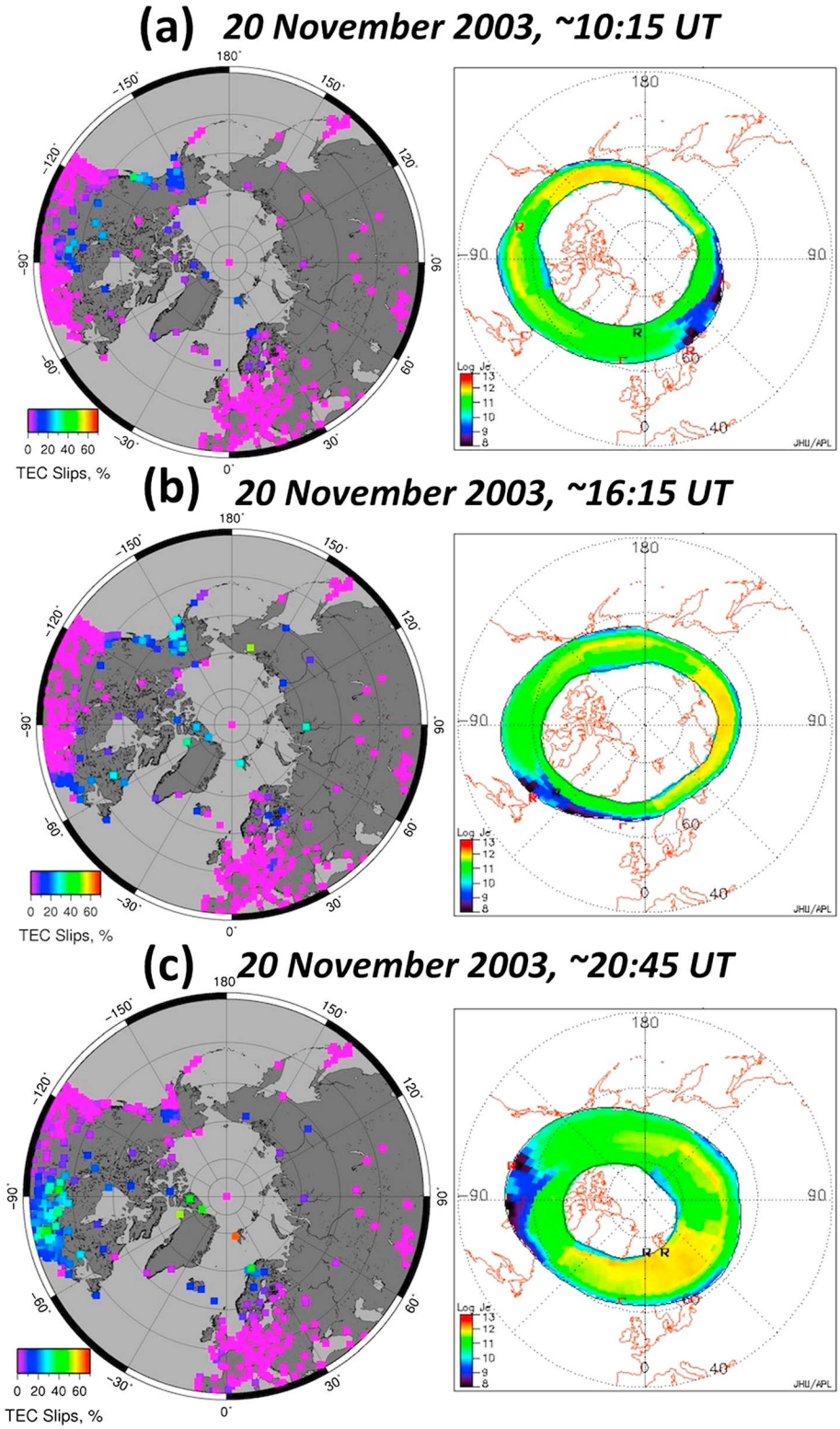

Figure 9. Polar view of the global maps of TEC slips occurred during the main phase of the super-storm of 20 November 2003 at (a) 10:15 UT, (b) ~16:15 UT, and (c) ~20:45 UT. Auroral ovals for these moments of time are shown on the right panels. According to OVATION, no DMSP or UVI data were available for these periods of time.

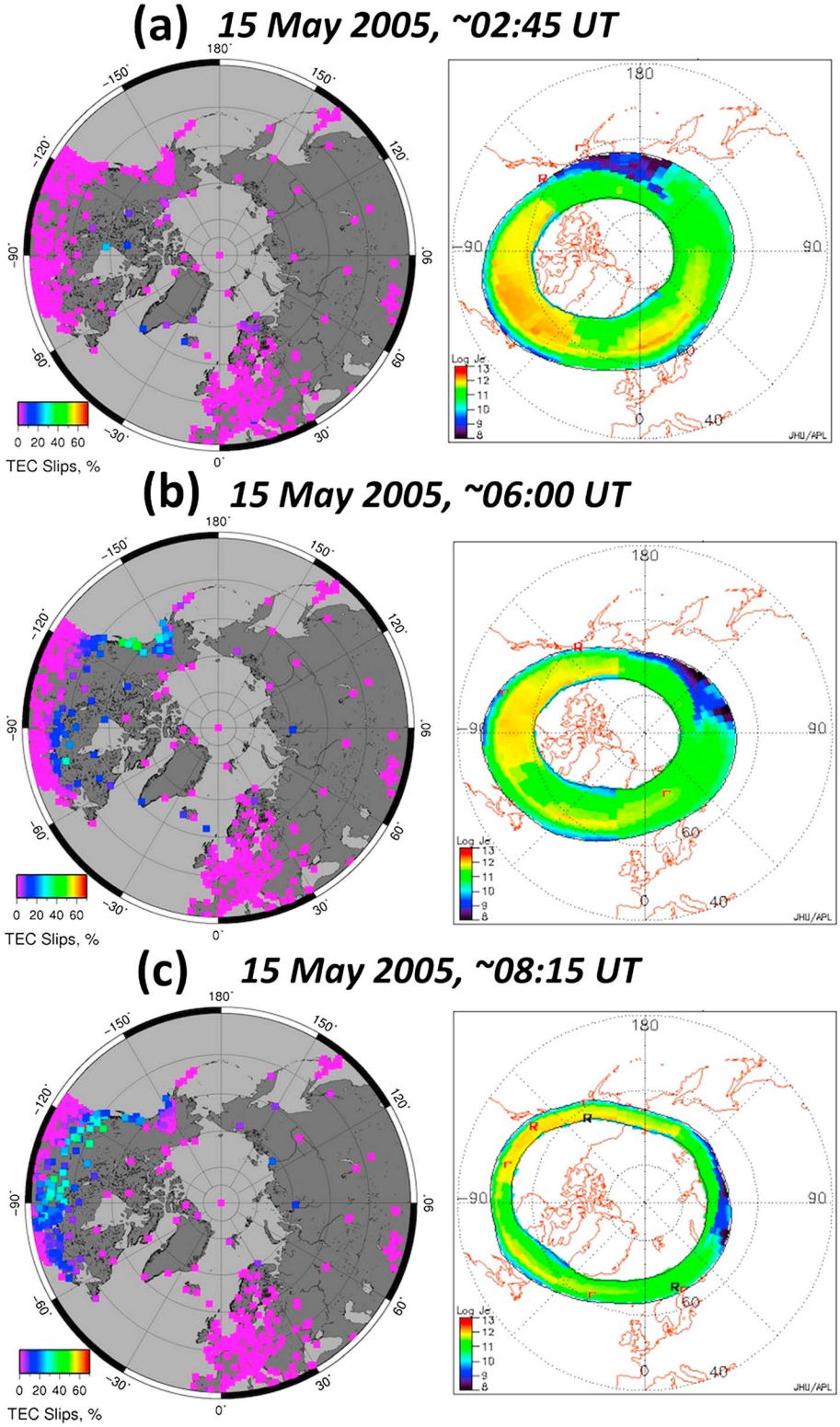

Figure 10. Polar view of the global maps of TEC slips occurred during the storm of 15 May 2005 at (a) ~02:45, (b) ~06:00, and (c) 08:15. Auroral ovals for these moments of time are shown on the right panels. According to OVATION, no DMSP or UVI data were available for these periods of time.

Acknowledgments
This work is supported by the European Research Council under the European Union's Seventh Framework Program (FP/2007–2013)/ERC Grant Agreement 307998. Yu. Ya. is supported by Russian Federation President Grant the RF President Grant MK-3771.2013.5. We cordially thank M. Mandea (CNES) for her support at the initial stage of this work. We thank the OMNIWeb Plus service (http://omniweb.gsfc.nasa.gov) for the geophysical and interplanetary data, and JHU/APL and the OVATION project for the maps of the auroral energy inputs. We acknowledge the reviewers for their valuable comments that helped to improve the manuscript.

References

Afraimovich, E. L., O. S. Lesyuta, I. I. Ushakov, and S. V. Voyeikov (2002), Geomagnetic storms and the occurrence of phase slips in the reception of GPS signals, *Ann. Geophys.*, *45*(1), 55–71.

Afraimovich, E. L., V. V. Demyanov, and T. N. Kondakova (2003), Degradation of performance of the navigation GPS system in geomagnetically disturbed conditions, *GPS Solutions*, *7*(2), 109–119.

Afraimovich, E. L., E. I. Astafieva, O. I. Berngardt, O. S. Lesyuta, V. V. Demyanov, T. N. Kondakova, and B. G. Shpynev (2004), Mid-latitude amplitude scintillation of GPS signals and GPS performance slips at the auroral oval boundary, *Radiophys. Quantum Electron.*, *47*(7), 453–468.

Afraimovich, E. L., V. V. Demyanov, A. B. Ishin, and G. Y. Smolkov (2008), Powerful radiobursts as a global and free tool for testing satellite broadband systems, including GPS-GLONASS-GALILEO, *J. Atm. Sol. Terr. Phys.*, *70*, 1985–1994.

Afraimovich, E. L., E. I. Astafyeva, V. V. Demyanov, and I. F. Gamayunov (2009), Mid-Latitude Amplitude Scintillation of GPS Signals and GPS Performance Slips, *Adv. Space Res.*, *43*(6), 964–972, doi:10.1016/j.asr.2008.09.015.

Afraimovich, E. L., E. I. Astafyeva, E. A. Kosogorov, and Y. V. Yasyukevich (2011), The mid-latitude field-aligned disturbances and their effects on differential GPS and VLBI, *Adv. Space Res.*, *47*(10), 1804–1813, doi:10.1016/j.asr.2010.06.030.

Astafyeva, E. (2009a), Effects of strong IMF Bz southward events on the equatorial and mid-latitude ionosphere, *Ann. Geophys.*, *27*, 1175–1187.

Astafyeva, E. I. (2009b), Dayside ionospheric uplift during strong geomagnetic storms as detected by the CHAMP, SAC-C, TOPEX and Jason-1 satellites, *Adv. Space Res.*, *43*, 1749–1756, doi:10.1016/j.asr.2008.09.036.

Astafyeva, E. I., E. L. Afraimovich, and E. A. Kosogorov (2007), Dynamics of total electron content distribution during strong geomagnetic storms, *Adv. Space Res.*, *39*, 1313–1317, doi:10.1016/j.asr.2007.03.006.

Astafyeva, E. I., E. L. Afraimovich, and S. V. Voeykov (2008), Generation of secondary waves due to intensive large-scale AGW traveling, *Adv. Space Res.*, *41*(9), 1459–1462, doi:10.1016/j.asr.2007.03.059.

Basu, S., S. Basu, F. J. Rich, K. M. Groves, E. MacKenzie, C. Coker, Y. Sahai, P. R. Fagundes, and F. Becker-Guedes (2007), Response of the equatorial ionosphere at dusk to penetration electric fields during intense magnetic storms, *J. Geophys. Res.*, *112*, A08308, doi:10.1029/2006JA012192.

Basu, S., S. Basu, J. J. Makela, E. MacKenzie, P. Doherty, J. W. Wright, F. Rich, M. J. Keskinen, R. E. Sheehan, and A. J. Coster (2008), Large magnetic storm-induced nighttime ionospheric flows at midlatitudes and their impacts on GPS-based navigation systems, *J. Geophys. Res.*, *113*, A00A06, doi:10.1029/2008JA013076.

Bergeot, N., C. Bruyninx, P. Defraigne, S. Pireaux, J. Legrand, E. Pottiaux, and Q. Baire (2011), Impact of the Halloween 2003 ionospheric storms on kinematic GPS positioning in Europe, *GPS Solutions*, *15*, 171–180, doi:10.1007/s10291-010-0181-9.

Dashora, N., S. Sharma, R. S. Dabas, S. Alex, and R. Pandey (2009), Large enhancements in low latitude total electron content during 15 May 2005 geomagnetic storm in Indian zone, *Ann. Geophys.*, *27*, 1803–1820, doi:10.5194/angeo-27-1803-2009.

de Abreu, A. J., et al. (2010), Hemispheric asymmetries in the ionospheric response observed in the American sector during an intense geomagnetic storm, *J. Geophys. Res.*, *115*, A12312, doi:10.1029/2010JA015661.

de Abreu, A. J., Y. Sahai, P. R. Fagundes, R. de Jesus, J. A. Bittencourt, and V. G. Pillat (2011), An investigation of ionospheric F region response in the Brazilian sector to the super geomagnetic storm of May 2005, *Adv. Space Res.*, *48*(7), 1211–1220, doi:10.1016/j.asr.2011.05.036.

de Jesus, R., Y. Sahai, F. L. Guarnieri, P. R. Fagundes, A. J. de Abreu, J. A. Bittencourt, T. Nagatsuma, C.-S. Huang, H. T. Lan, and V. G. Pillat (2012), Ionospheric response of equatorial and low latitude F-region during the intense geomagnetic storm on 24–25 August 2005, *Adv. Space Res.*, *49*(3), 518–529, doi:10.1016/j.asr.2011.10.020.

de Paula, E. R., F. S. Rodriguez, K. N. Iyer, I. J. Kantor, M. A. Abdu, P. M. Kintner, B. M. Ledvina, and H. Kil (2003), Equatorial effects on GPS scintillations in Brazil, *Adv. Space Res.*, *31*(3), 749–754, doi:10.1016/S0273-1177(03)00048-6.

Demyanov, V. V., Y. V. Yasukevich, A. B. Ishin, and E. I. Astafyeva (2012), Effects of ionosphere super-bubble on GPS performance depending on the bubble orientation relative to geomagnetic field, *GPS Solutions*, *16*(2), 181–189, doi:10.1007/s10291-011-0217-9.

Doherty, P. H., S. H. Delay, C. E. Valladares, and J. A. Klobuchar (2001) Ionospheric scintillation effects in the equatorial and auroral regions, in *Proceedings of International Beacon Satellite Symposium, June 4–6*, pp. 328–333, Boston College, Institute for Scientific Research, Chestnut Hill, Mass.

Foster, J. C., and A. J. Coster (2007), Conjugate localized enhancement of total electron content at low latitudes in the American sector, *J. Atmos. Sol. Terr. Phys.*, *69*, 1241–1252.

Foster, J. C., and W. Rideout (2005), Midlatitude TEC enhancements during the October 2005 superstorm, *Geophys. Res. Lett.*, *32*, L12S04, doi:10.1029/2004GL021719.

Jakowski, N., S. M. Stankov, and D. Klaehn (2005), Operational space weather service for GNSS precise positioning, *Ann. Geophys.*, *23*, 3071–3079.

Jakowski, N., C. Mayer, V. Wilken, and C. Borries (2007), Ionospheric storms at high and mid-latitudes monitored by ground and space based GPS techniques, in *Proceedings of the International Beacon Satellite Symposium, June 11–15, 2007*, edited by P. H. Doherty, Boston College, Chestnut Hill, Mass.

Kelley, M. C., J. J. Makela, J. L. Chau, and M. J. Nicolis (2003), Penetration of the solar wind electric field into the magnetosphere/ionosphere system, *Geophys. Res. Lett.*, *30*(4), 1158, doi:01.1029/2002GL016321.

Kelley, M. C., R. R. Ilma, M. Nicolis, P. Erickson, L. Goncharenko, J. L. Chau, N. Appointe, and J. U. Kozyra (2010), Spectacular low- and mid-latitude electric fields and neutral winds during a superstorm, *J. Atmos. Sol. Terr. Phys.*, *72*, 285–291.

Ledvina, B. M., J. J. Makela, and P. M. Kintner (2002), First observations of intense GPS L1 amplitude scintillations at mid-latitude, *Geophys. Res. Lett.*, *29*(14), 1659, doi:10.1029/2002GL014770.

Ma, G., and T. Maruyama (2006), A super bubble detected by dense GPS network at east Asian longitudes, *Geophys. Res. Lett.*, *33*, L21103, doi:10.1029/2006GL027512.

Mannucci, A. J., B. T. Tsurutani, B. A. Iijima, A. Komjathy, A. Saito, W. D. Gonzalez, F. L. Guarnieri, J. U. Kozyra, and R. Skoug (2005), Dayside global ionospheric response to the major interplanetary events of October 29–30, 2003 "Halloween Storms", *Geophys. Res. Lett.*, *32*, L12S02, doi:10.1029/2004GL021467.

Mannucci, A. J., B. T. Tsurutani, M. A. Abdu, W. D. Gonzalez, A. Komjathy, E. Echer, B. A. Iijima, G. Crowley, and D. Anderson (2008), Superposed epoch analysis of the dayside ionospheric response to four intense geomagnetic storms, *J. Geophys. Res.*, *113*, A00A02, doi:10.1029/2007JA012732.

Mannucci, A. J., B. T. Tsurutani, M. C. Kelley, B. A. Iijima, and A. Komjathy (2009), Local time dependence of the prompt ionospheric response for the 7, 9, and 10 November 2004 superstorms, *J. Geophys. Res.*, *114*, A10308, doi:10.1029/2009JA014043.

Mannucci, A. J., G. Crowley, B. T. Tsurutani, O. P. Verkhoglyadova, A. Komjathy, and P. Stephens (2014), Interplanetary magnetic field by control of prompt total electron content increases during superstorms, *J. Atm. Solar Terr. Phys.*, *115–116*, 7–16, doi:10.106/j.jastp.2014.01.001.

Ngwira, C. M., L.-A. McKinnell, P. J. Cilliers, and E. Yizangaw (2012), An investigation of ionospheric disturbances over South Africa during the magnetic storm on 15 May 2005, *Adv. Space Res.*, *49*(2), 327–335, doi:10.1016/j.asr.2011.09.035.

Nishioka, M., A. Saito, and T. Tsugawa (2009), Super-medium-scale traveling ionospheric disturbance observed at midlatitude during the geomagnetic storm on 10 November 2004, *J. Geophys. Res.*, *114*, A07310, doi:10.1029/2008JA013581.

Paznukhov, V. V., D. Altadill, and B. W. Reinisch (2009), Experimental evidence for the role of the neutral wind in the development of ionospheric storms in midlatitudes, *J. Geophys. Res.*, *114*, A12319, doi:10.1029/2009JA014479.

Pi, X., A. J. Mannucci, U. J. Lindqwister, and C. M. Ho (1997), Monitoring of global ionospheric irregularities using the worldwide GPS network, *Geophys. Res. Lett.*, *24*(18), 2283–2286, doi:10.1029/97GL02273.

Pi, X., B. M. Boulat, B. J. Iijima, A. J. Mannucci, and D. A. Stowers (2002), *Latitudinal Characteristics of L-band Ionospheric Scintillation*, ION-GPS, Portland, Oregon.

Pi, X., A. Freeman, B. Chapman, P. Rosen, and Z. Li (2011), Imaging ionospheric inhomogeneities using spaceborne synthetic aperture radar, *J. Geophys. Res.*, *116*, A04303, doi:10.1029/2010JA016267.

Pi, X., A. J. Mannucci, B. Valant-Spraight, Y. Bar-Sever, L. J. Romans, S. Skone, L. Sparks, and G. Martin Hall (2013), Observations of Global and Regional Ionospheric Irregularities and Scintillations using GNSS tracking networks, in *Proceedings of ION Pacific PNT Conference*, pp. 752–761, Honolulu, Hawaii, 22–25 April 2013, Jet Propulsion Laboratory, National Aeronautics and Space Administration, Pasadena, Calif.

Rama Rao, P. V. S., S. Gopi Krishna, J. Vara Prasad, S. N. V. S. Prasad, D. S. V. V. D. Prasad, and K. Niranjan (2009), Geomagnetic storm effects on GPS based navigation, *Ann. Geophys.*, *27*, 2101–2110.

Skone, S., and M. de Jong (2000), The impact of geomagnetic substorms on GPS receiver performance, *Earth Planets Space*, *52*, 1067–1071.

Skone, S., and M. de Jong (2001), Limitations in GPS receiver tracking performance under ionospheric scintillations, *Phys. Chem. Earth. Part A*, *26*(6–8), 613–621.

Tsurutani, B., et al. (2004), Global dayside ionospheric uplift and enhancement associated with interplanetary electric fields, *J. Geophys. Res.* *109*, A08302, doi:10.1029/2003JA010342.

Yeh, K. C., and C. H. Liu (1982), Radio wave scintillations in the ionosphere, *Proc. IEEE*, *70*, 324.

Zhao, B., et al. (2008), Ionosphere disturbances observed throughout Southeast Asia of the superstorm of 20–22 November 2003, *J. Geophys. Res.*, *113*, A00A04, doi:10.1029/2008JA013054.